Dynamics of aqueous ferrofluid droplets at coflowing liquid-liquid interface under a non-uniform magnetic field

U. Banerjee, A. Raj, and A. K. Sen

Citation: Appl. Phys. Lett. **113**, 143702 (2018); doi: 10.1063/1.5046332
View online: https://doi.org/10.1063/1.5046332
View Table of Contents: http://aip.scitation.org/toc/apl/113/14
Published by the American Institute of Physics

Dynamics of aqueous ferrofluid droplets at coflowing liquid-liquid interface under a non-uniform magnetic field

U. Banerjee, A. Raj, and A. K. Sen[a)]
Department of Mechanical Engineering, Indian Institute of Technology Madras, Chennai 600036, India

(Received 27 June 2018; accepted 20 September 2018; published online 3 October 2018)

We report the dynamical behaviour of aqueous ferrofluid droplets (FFDs) of different sizes and concentrations at the interface of coflowing immiscible oils in a microchannel in the presence of the magnetic field. We show that the migration and sorting phenomena are governed by the interplay between magnetic force F_m, non-inertial lift force F_l, and interfacial tension force F_i. Depending on the force ratios, namely, the lift force ratio $[K_L = (F_l/F_i)]$ and magnetic force ratio $[K_M = (F_m/F_i)]$, three different regimes are identified. The results also reveal that the FFD trajectory and migration length (L^*_{mig}) depend on the net force ratio $[F_{R,net} = ((F_m + F_l)/F_i)]$ and magnet location x^*_m. Finally, size-based sorting of FFD is demonstrated, which shows a remarkable improvement in terms of the size range and resolution compared to when the magnetic field is not present. *Published by AIP Publishing*. https://doi.org/10.1063/1.5046332

Precise manipulation of droplets is of significant interest to the microfluidic community. Incessant progress in droplet manipulation has played a vital role in the rapid development in cell sorting,[1] disease detection,[2] and chemical reactions.[3] Depending on the applications, droplet manipulation can be either continuous or discrete. Continuous manipulation[4] embraces a large quantity of droplets to be manipulated in closed microfluidic channels and discrete manipulation involves droplet manipulation on open engineered surfaces.[5–8] Manipulation techniques can be classified as active and passive. Active techniques use external stimuli such as light,[9,10] Electrowetting-on-dielectric (EWOD),[11,12] and magnetic field[13] to actuate droplets in contrast to passive techniques, where surface morphology[14,15] and flow dynamics[16,17] play the utmost role. Considering the pros and cons of various active techniques, magnet-based manipulation has gained immense importance due to its simplicity and low-cost. It facilitates contact free manipulation of magnetic[18] as well as non-magnetic droplets,[19] particles,[20] and cells[21] on both continuous and digital microfluidic platforms. Magnetic droplets can be concocted from an aqueous solution containing magnetic particles or using commercially available ferrofluids.[22] The breakup dynamics of ferrofluid droplet (FFD) inside a T-junction microchannel[23] and flow focusing device[24] in the presence of uniform and non-uniform magnetic fields has been studied. It is found that the breakup process and frequency can be easily modulated using a uniform magnetic field as compared to a non-uniform magnetic field.

The literature clearly shows that there is limited understanding of the interaction between FFD and liquid interfaces since most of the reported literature studies discuss FFD manipulation in a single continuous phase. It includes the influence of the uniform magnetic field on various droplet generation regimes,[25] sizes, and frequencies,[26] which reports the periodic generation of ferrofluid droplets of various sizes using the square wave magnetic field. Another study[27] depicts the influence of the uniform magnetic field on the ferrofluid droplet size, shape, inter droplet spacing, and velocity by varying the magnetic susceptibility of the FF, continuous phase viscosity, and flow rates. Dynamics of aqueous droplets at the liquid-liquid interface is well comprehended in the literature,[28–30] where the shear rate is used as the key parameter to sort aqueous droplets of various sizes and deformability. However, such a system uses high-viscous liquids. It is extremely challenging to vary and control the shear rate in such liquids to control the droplet size range and sorting resolution. The present study accounts such issues by enabling the manipulation of FFD using an external agent (nonuniform magnetic field), which shows enhancement in the sorting range, improvement in the sorting resolution, and control over the migration length.

Figure 1 delineates the schematic of FFD migration across coflowing immiscible continuous phases CP_1 and CP_2 in the presence and absence of a non-uniform magnetic field. The Reynold's number in our case $Re \ll 1$, which bolsters the fact that non-inertial lift[31,32] $F_l = C_l \frac{\mu_{CP}\dot{\gamma}R^3}{y}$ will be predominant and steering the lateral migration of FFD, where $\dot{\gamma}$ is the shear rate, R is the FFD radius, μ_{CP} is the continuous phase viscosity, y is the lateral position from the wall, and C_l is the lift coefficient dependent on FFD orientation, viscosity ratio, and radius.

At low Re, owing to the object size and deformability, shear rate, orientation, viscosity ratio, and lateral position of the object with respect to the channel wall, deformable objects such as droplets and vesicles experience non-inertial lift, due to which such objects tend to achieve the minimum shear zone (where velocity is maximum) as reported in the literature.[28] In the case of a single-phase fluid flow, the minimum zone resides at the channel centerline. However, in the case of coflowing liquids, the minimum shear zone exists inside the low viscosity liquid which leads to two different possibilities—a droplet will either remain in the CP_1 or may penetrate the interface to reach the minimum shear zone in CP_2. In the present case, the non-inertial lift force acts on an

[a)]Author to whom correspondence should be addressed: ashis@iitm.ac.in

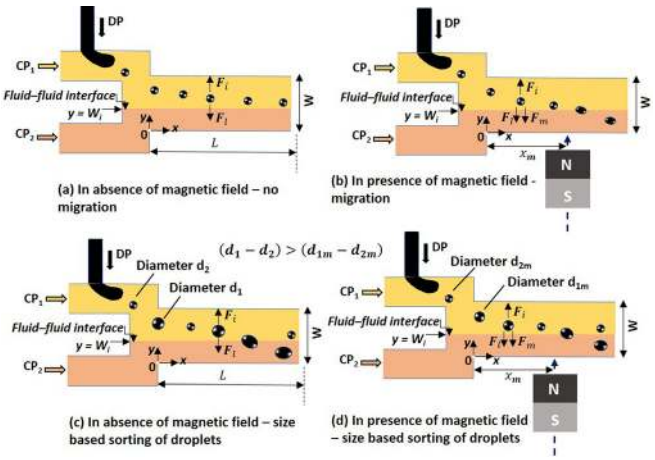

FIG. 1. Schematic of the experimental device showing non-migration and migration of ferrofluid droplets (FFDs) across the interface of co-flowing fluids (CP_1 and CP_2) in the absence (a) and presence (b) of the magnetic field, respectively. Size based sorting of droplets in the (c) absence and (d) presence of the magnetic field; the magnetic field improves sorting resolution; d_1 and d_2 are diameters of larger and smaller droplets in the absence of the magnetic field, and d_{1m} and d_{2m} are the diameters of larger and smaller droplets in the presence of the magnetic field, $(d_1 - d_2) > (d_{1m} - d_{2m})$ magnetic field improves sorting resolution.

object present at any arbitrary location in CP_1 toward the minimum shear zone (in CP_2).

The later situation requires the following two conditions be satisfied—(i) The droplet comes in contact with the interface due to sufficient non-inertial lift within the available channel length and (ii) the non-inertial lift is sufficient to overcome the interfacial tension (IFT)[28,33] $F_i \sim \sigma R$ offered by the interface between CP_1 and CP_2, where σ is the interfacial tension between CP_1 and CP_2. While larger FFDs that are subjected to higher non-inertial lift or immiscible continuous phases with a smaller IFT would satisfy the above two conditions and migrate across the interface, manipulation of smaller FFDs or continuous phases of higher IFTs would require an external field. In such scenarios, a combination of non-inertial lift force F_i and magnetic force[34,35] $F_m = \frac{n\Delta\chi V_p}{\mu_0} B\nabla B$ can cause migration of FFD across the interface within the available length, n—number of magnetic nanoparticles $(\approx 6.8 \times 10^{23}\ \text{particles/m}^3)$ for pure ferrofluid, $\Delta\chi$—difference in magnetic susceptibility of the magnetic nanoparticle and the buffer $(\approx 10^{-3})$, V_p—volume of each nanoparticle (m^3), μ_0—permeability of free space $(4\pi \times 10^{-7}\ \text{H/m})$, B—magnetic flux density (T), and ∇B—gradient of magnetic flux density (T/m). FFD migration in the presence of the magnet and non-migration in the absence of the magnet can be seen in supplementary videos VS1 and VS2, respectively.

The microchannel device was fabricated in Polydimethylsiloxane (PDMS) by following the standard soft lithography procedure.[17] We have used microchannels of widths 300, 500, and 800 μm and depth 100 μm. Silicone oil AP1000 (Sigma-Aldrich, Bangalore, India) was used as the primary continuous phase (CP_1) and mineral oil (Sigma-Aldrich, Bangalore, India) was used as the secondary continuous phase (CP_2). In our experiments, we have used a commercial water based ferrofluid (EMG 408, Ferrotec, Singapore) with glycerol (glycerol 0–40% v/v) (Sigma-Aldrich, Bangalore, India) as the discrete phase. The properties of ferrofluid[7] and the oils[28] used in the experiments are mentioned elsewhere.[7,28] A neodymium iron boron (NdFeB) permanent magnet $(L = W = H = 0.47\ \text{cm})$ (K&J Magnetics, Inc., USA) was used for the experiments. The magnetic flux density of the permanent magnet is provided in the supplementary material (Fig. S1). The continuous and discrete phases are supplied using 2.5 ml plastic syringes (Dispovan) equipped on syringe pumps (neMESYS Pump, Cetoni, Germany). The interface location and FFD motion are captured using an inverted microscope (Olympus) coupled with a high-speed camera operating at 1000 fps (FASTCAM SA4 model, Photron USA, Inc.) interfaced with a Personal Computer (PC) via Photron Fastcam Viewer software.

The interplay between three different forces F_l, F_i, and F_m decides the final destination of FFD in the microchannel. The phenomenon of FFD migration can be characterized based on two force ratios: lift force ratio $K_L = (F_l/F_i)$ and magnetic force ratio $K_M = (F_m/F_i)$, which depict the various regimes of FFD transport, as shown in Fig. 2(a).

The "no migration regime" depicts (black square) that FFD migration is not observed for $K_L \leq 0.44$ and $0 \leq K_M \leq 0.14$, which can be attributed to insufficient non-inertial lift F_l and magnetic force F_M due to the smaller size $(K_L \sim R^2, K_M \sim R^2)$, low strain rate $(K_L \sim \dot{\gamma})$, less deformability $(K_L \sim C_l)$, and lower concentration $(K_M \sim n)$. If we keep strain rate and % glycerol fixed, both K_L and K_M are found to increase with the increase in the FFD size. Similarly, for the fixed size and strain rate, increase in % glycerol results in an increase in K_L due to the increment in deformability and decrease in K_M due to the reduction in the particle concentration. The combination of these two effects leads the FFDs into a different regime known as "partial migration regime" (red circles), which is defined for $0.44 < K_L \leq 0.46$ and $0.14 < K_M \leq 0.16$.

Further increment in size and % glycerol enhances both the force ratios leading to the complete migration of FFD. The "migration regime" (blue triangles) spreads over a wide region defined by $K_L > 0.46$ or/and $K_M > 0.16$. In the absence of magnetic force $(K_M = 0, K_L = 0.34)$, FFD migration is not observed as shown in Fig. 2(b) which falls within the defined limit as mentioned above. As soon as the magnetic force comes into play, FFD starts to deflect toward

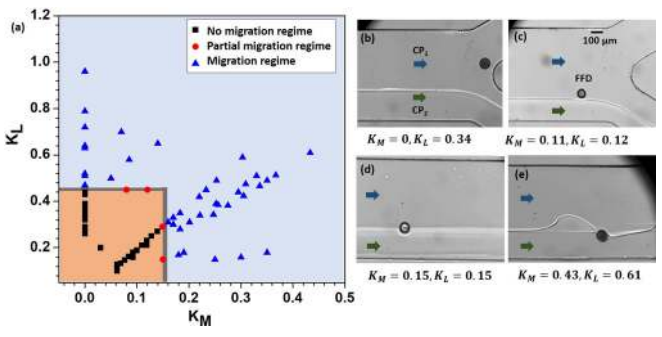

FIG. 2. (a) Regimes (no migration, partial migration, and migration) of FFD transport based on non-inertial lift and magnetic force ratios; (b)–(e) pictorial illustration of various cases (no-migration, no-migration but FFD rolling over interface, partial migration, and migration, respectively) depicting different regimes showing FFD migration inside a microchannel of outlet width $(W = 800\ \mu\text{m})$.

the interface, which is seen in Figs. 2(c) and 2(d). Due to insufficient K_L and K_M, droplet rolls over the interface in (c) as compared to partial migration in (d). When both the ratios K_M and K_L are higher (i.e., sum of magnetic and non-inertial lift exceeds the interfacial tension force), the FFD completely migrates and locate itself at the minimum shear zone (in CP_2), as observed in (e). During interfacial migration, the competition between the forces leads to instability (waviness) at the interface [see Fig. 2(e)], which has also been reported in the literature[28,36] for water and liquid metal droplets. We also observed that once the droplet completely migrates into the CP_2, the interface becomes stable (flat) again.

Figure 3 shows the effect of net force ratio $F_{R,net} = [(F_m + F_l)/F_i]$ and magnet location x_m^* on the migration length L_{mig}^* of FFD. Experiments are performed with FFDs of various concentrations and sizes in the presence of the magnetic field to estimate the migration length L_{mig}^*. The gap (g) between the channel wall and the magnet surface is kept fixed at $g = 1$ mm throughout the experiments. The position of the magnet is varied in each case (i.e., x_m^*) along the x-direction (Fig. 1). Co-ordinates corresponding to magnet centre x_m and the FFD migration location L_{mig} (at which the FFD completely enters CP_2) are non-dimensionalised by the channel length $(L = 2.7$ cm) to get $x_m^* = (x_m/L)$ and $L_{mig}^* = \left(L_{mig}/L\right)$, respectively. The net force ratio $F_{R,net}$ is defined as the summation of non-inertial lift and magnetic force ratios $F_{R,net} = (K_L + K_M)$. It is found from Fig. 3(a) that when $x_m^* = 0.55$ and $F_{R,net} = 0.58$, the FFD migrates at $L_{mig}^* = 0.66$, and when $x_m^* = 0.55$ and $F_{R,net} = 0.62$, the migration occurs at $L_{mig}^* = 0.63$. Similarly, FFD migration happens at $L_{mig}^* = 0.51$ in the case of $x_m^* = 0.35$, $F_{R,net} = 0.82$ as compared to $x_m^* = 0.35$, $F_{R,net} = 0.91$ in which $L_{mig}^* = 0.49$. The shorter migration length can be attributed to increase in size or higher % glycerol due to which the net force ratio $(F_{R,net} \sim R^2)$ increases. Figure 3(b) depicts the control of FFD migration length by positioning the magnet at a particular location, e.g., if we compare the migration of FFDs for which $F_{R,net} = 0.82$, we found that for a magnet location $x_m^* = 0.35$, the migration of FFD occurs at $L_{mig}^* = 0.51$, and for $x_m^* = 0.40$, the migration happens at $L_{mig}^* = 0.53$, which shows the control of the migration length by locating the magnet at a particular position.

Finally, in Fig. 4, we demonstrate a wider size range and smaller resolution in the case of magnetic assisted sorting of

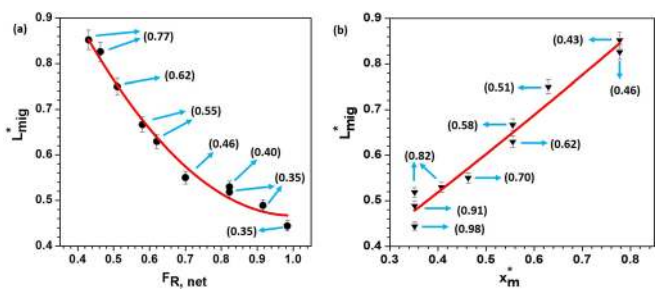

FIG. 3. (a) Variation of the non-dimensional migration length (L_{mig}^*) with net force ratio $(F_{R,net})$ for various FFD migration cases; (b) variation of non-dimensional migration length (L_{mig}^*) with various magnet locations (x_m^*); the inset values in the plot represent the corresponding x_m^* in (a) and corresponding $F_{R,net}$ in (b).

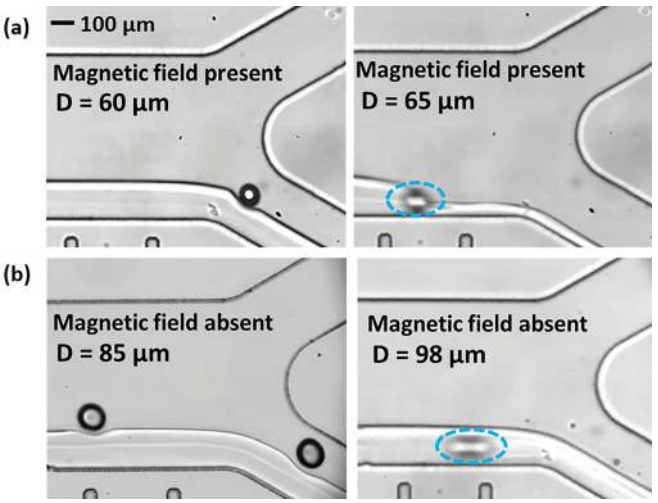

FIG. 4. (a) Size based sorting of FFDs of size $D = 65\mu$m and $D = 60\mu$m in the presence of the magnetic field; (b) size based sorting of FFDs of size $D = 85\mu$m and $D = 98\mu$m in the absence of the magnetic field, in both cases of channel outlet width $W = 500\mu$m and interface location $W_i^* = 0.78$.

FFD as compared to non-magnetic manipulation. FFDs of different sizes are generated by controlling the discrete phase (FF) flow rate, keeping the continuous phase flow rates the same. For a fixed interface location $W_i^* = 0.78$ and pure ferrofluid (0% glycerol), we generated droplets of size $D = 60\,\mu$m and $D = 65\,\mu$m in CP_1, where $W_i^* = (W - W_i)/W$. In the presence of the magnetic field, droplets of size $D = 60\,\mu$m do not migrate into CP_2 and simply roll over the interface. On the contrary, larger size FFDs $(D = 65\,\mu$m) migrate into CP_2, as shown in Fig. 4(a) [see supplementary video (VS3)]. This can be argued on the basis of the net force ratio being higher in the case of larger size FFD $(D = 65\,\mu$m) as compared to smaller size FFD $(D = 60\,\mu$m) which results in its migration. Similarly, in Fig. 4(b), for fixed interface location $W_i^* = 0.78$ and pure ferrofluid (0% glycerol), we generated FFD of size $D = 85\,\mu$m and $D = 98\,\mu$m in CP_1. In the absence of the magnetic field, droplet trajectory is governed by the non-inertial lift alone. Due to insufficient lift force, even FFD of size $D = 85\,\mu$m are unable to migrate across the interface and simply roll over the interface whereas only FFD of size $D = 98\,\mu$m migrate into CP_2 [see supplementary video (VS4)]. The FFD of size between $D = 60\,\mu$m and $D = 65\,\mu$m in the presence of the magnetic field and FFD of size between $D = 85\,\mu$m and $D = 98\,\mu$m in the absence of the magnetic field exhibit partial migration. The above shows two strong features of using a magnetic field for FFD manipulation. First, the size range in which FFDs migrate into CP_2 is significantly wider in the case of magnetic manipulation as compared to non-magnetic manipulation, thus enabling magnetic sorting of FFD of a wider range of sizes.

Second, the resolution of FFD manipulation is $\sim 5\,\mu$m using a magnetic field but is $>10\,\mu$m in the case of non-magnetic manipulation. The enhancement in sorting resolution in the case of magnetic assisted manipulation can be explained as follows—when the FFD manipulation is due to non-inertial lift alone, due to increment in size the lift force ratio modifies from $(F_L/F_i) = \alpha R^2$ to $(F_L/F_i) = \alpha(R + \Delta R)^2$, where α is a positive constant for a particular strain rate and liquid

combination. In the case of magnetic assisted manipulation, increment in FFD size modifies the net force ratio from $(F_L + F_M)/F_i = (\alpha + \beta)R^2$ to $(F_L + F_M)/F_i = (\alpha + \beta)(R + \Delta R)^2$, where β is also a positive constant for a particular magnet strength and liquid combination. This verifies the fact that the resolution of magnetic assisted sorting is better as compared to pure non-inertial lift based sorting owing to the higher net force ratio for a small difference in the FFD size (ΔR).

In summary, we reported the physics behind the manipulation of aqueous ferrofluid droplets (FFD) of different sizes and concentrations at the interface of coflowing immiscible liquids in a microchannel in the presence of the magnetic field. The interplay between magnetic force F_m, non-inertial lift force F_l, and interfacial tension force F_i governs the interfacial migration of FFD. Three different regimes, namely, "no migration," "partial migration," and "migration" were observed depending on the force ratios, namely, the lift force ratio $[K_L = (F_l/F_i)]$ and magnetic force ratio $[K_M = (F_m/F_i)]$. Migration lengths of FFDs are found to reduce with net force ratio $F_{R,net} = K_L + K_M$ and increase with magnet location x_m^*, which shows that controlled manipulation of FFD is possible. Finally, sorting of FFDs of various sizes and concentrations is elucidated. It was observed that the migration range of FFDs is widened in the case of magnetic manipulation as compared to non-magnetic manipulation. Also, the size resolution of FFD sorting is significantly improved in the case of magnetic manipulation $(\sim 5\,\mu\text{m})$ in comparison to non-magnetic manipulation $(>10\,\mu\text{m})$. It is found that whenever FFD tries to migrate from CP_1 to CP_2, it perturbs the interface which results in an instability (wavy interface) and after migration the interface becomes stable (flat) again. This behaviour does not affect the droplet migration behaviour as far as the generation frequency is not too high.

See supplementary material for distribution of magnetic flux density of magnet and supplementary video for migration (VS1) and non-migration of FFD (VS2), size-based sorting in the presence (VS3) and absence (VS4) of magnetic field.

This work was supported by the Science and Engineering Research Board (SERB), the Department of Science and Technology (DST), India, via Grant No. EMR/2014/001151, and the IIT Madras via Project No. MEE1516843RFTPASHS.

[1]W. Zhao, R. Cheng, B. D. Jenkins, T. Zhu, N. E. Okonkwo, C. E. Jones, M. B. Davis, S. K. Kavuri, Z. Hao, C. Schroeder, and L. Mao, Lab Chip **17**, 3097–3111 (2017).
[2]Y. Zhang, S. Park, K. Liu, J. Tsuan, S. Yang, and T.-H. Wang, Lab Chip **11**, 398 (2011).
[3]H. Song, D. L. Chen, and R. F. Ismagilov, Angew. Chem., Int. Ed. **45**, 7336 (2006).
[4]B. Teste, N. Jamond, D. Ferraro, J. L. Viovy, and L. Malaquin, Microfluid. Nanofluid. **19**, 141 (2015).
[5]N. T. Nguyen, G. Zhu, Y. C. Chua, V. N. Phan, and S. H. Tan, Langmuir **26**, 12553 (2010).
[6]A. Egatz-Gómez, S. Melle, A. A. García, S. A. Lindsay, M. Márquez, P. Domínguez-García, M. A. Rubio, S. T. Picraux, J. L. Taraci, T. Clement, D. Yang, M. A. Hayes, and D. Gust, Appl. Phys. Lett. **89**, 034106 (2006).
[7]U. Banerjee and A. Sen, Soft Matter **14**, 2915–2922 (2018).
[8]P. Irajizad, N. Farokhnia, and H. Ghasemi, Appl. Phys. Lett. **107**, 191601 (2015).
[9]P. Y. Chiou, S. Y. Park, and M. C. Wu, Appl. Phys. Lett. **93**, 221110 (2008).
[10]D. Jiang and S.-Y. Park, Lab Chip **16**, 1831 (2016).
[11]M. Jönsson-Niedziółka, F. Lapierre, Y. Coffinier, S. J. Parry, F. Zoueshtiagh, T. Foat, V. Thomy, and R. Boukherroub, Lab Chip **11**, 490 (2011).
[12]J. Lee, H. Moon, J. Fowler, T. Schoellhammer, and C. J. Kim, Sens. Actuators, A **95**, 259 (2002).
[13]G. Katsikis, A. Bréant, and M. Prakash, Soft Matter **14**, 681–692 (2017).
[14]M. H. Alheshibri, N. G. Rogers, A. D. Sommers, and K. F. Eid, Appl. Phys. Lett. **102**, 174103 (2013).
[15]Y. Zheng, J. Cheng, C. Zhou, H. Xing, X. Wen, P. Pi, and S. Xu, Langmuir **33**, 4172 (2017).
[16]B.-J. Jin, Y. W. Kim, Y. Lee, and J. Y. Yoo, J. Micromech. Microeng. **20**, 035003 (2010).
[17]P. Sajeesh, M. Doble, and A. K. Sen, Biomicrofluidics **8**, 054112 (2014).
[18]A. Ray, V. B. Varma, P. J. Jayaneel, N. M. Sudharsan, Z. P. Wang, and R. V. Ramanujan, Sens. Actuators, B **242**, 760 (2017).
[19]S. Damodara and A. K. Sen, Sens. Actuators, B **239**, 816 (2017).
[20]Q. Chen, D. Li, J. Lin, M. Wang, and X. Xuan, Anal. Chem. **89**, 6915 (2017).
[21]T. Zhu, R. Cheng, S. A. Lee, E. Rajaraman, M. A. Eiteman, T. D. Querec, E. R. Unger, and L. Mao, Microfluid. Nanofluid. **13**, 645 (2012).
[22]C. Y. Chen and Z. Y. Cheng, Phys. Fluids **20**, 054105 (2008).
[23]Y. Wu, T. Fu, Y. Ma, and H. Z. Li, Microfluid. Nanofluid. **18**, 19 (2015).
[24]Y. Wu, T. Fu, Y. Ma, and H. Z. Li, Soft Matter **9**, 9792 (2013).
[25]T. S. Sheu, Y. T. Chen, F. L. Lih, and J. M. Miao, Phys. Procedia **9**, 147 (2010).
[26]Q. Yan, S. Xuan, X. Ruan, J. Wu, and X. Gong, Microfluid. Nanofluid. **19**, 1377 (2015).
[27]V. B. Varma, A. Ray, Z. Wang, Z. Wang, R. Wu, P. J. Jayaneel, N. M. Sudharsan, and R. V. Ramanujan, IEEE Magn. Lett. **7**, 2105305 (2016).
[28]K. S. Jayaprakash, U. Banerjee, and A. K. Sen, Langmuir **32**, 2136 (2016).
[29]A. C. DeVoria and K. Mohseni, Phys. Fluids **27**, 012002 (2015).
[30]M. Manga and H. A. Stone, J. Fluid Mech. **287**, 279 (1995).
[31]M. Abkarian, C. Lartigue, and A. Viallat, Phys. Rev. Lett. **88**, 068103 (2002).
[32]G. Coupier, B. Kaoui, T. Podgorski, and C. Misbah, Phys. Fluids **20**, 111702 (2008).
[33]Y. Couder, E. Fort, C. H. Gautier, and A. Boudaoud, Phys. Rev. Lett. **94**, 177801 (2005).
[34]K. Zhang, Q. Liang, S. Ma, X. Mu, P. Hu, Y. Wang, and G. Luo, Lab Chip **9**, 2992 (2009).
[35]N. Pamme and A. Manz, Anal. Chem. **76**, 7250 (2004).
[36]B. Gol, F. J. Tovar-Lopez, M. E. Kurdzinski, S.-Y. Tang, P. Petersen, A. Mitchell, and K. Khoshmanesh, Lab Chip **15**, 2476 (2015).